

Eco-friendly mechanochemical synthesis of titania-graphene nanocomposites for pesticide photodegradation

Viviana Jehová González,^{*a} Ester Vázquez,^{a,b} Beatriz Villajos,^c Alvaro Tolosana-Moranchel,^d Carlos Duran-Valle,^e Marisol Faraldos,^c Ana Bahamonde^{*c}

^a Instituto Regional de Investigación Científica Aplicada (IRICA), UCLM, 13071 Ciudad Real, Spain

^b Facultad de Ciencias y Tecnologías Químicas, UCLM, Avda. Camilo José Cela S/N, 13071, Ciudad Real, Spain

^c Environmental Catalysis Engineering Group, Instituto de Catálisis y Petroleoquímica, ICP-CSIC, Marie Curie 2, 28049 Madrid, Spain

^d Nanotechnology and Integrated BioEngineering Centre, School of Engineering, Ulster University, Northern Ireland, BT37 0QB, United Kingdom

^e IACYS, Universidad de Extremadura, Av. Elvas S/N, 06006 Badajoz (Spain).

Abstract

A mechanochemical treatment, starting from graphite and TiO₂ precursors in a simple and sustainable approach, has led to the preparation of titania graphene hybrid nanocomposites (TiO₂-FLG) as efficient nano-catalysts for photocatalytic degradation of a complex mixing of pesticides (isoproturon, pyrimethanil, alachlor and methomyl). The effect of few layer graphene (FLG) loading (0-1.0%) was analyzed to define the optimal ratio of FLG to TiO₂ and compared with the corresponding physical mixtures. X-ray Powder Diffraction (XRD) patterns of all these hybrid photocatalysts have presented the same crystal structure, with anatase as the main crystalline phase and brookite as secondary phase. An interaction between the graphene structure and the TiO₂ nanoparticles has been observed from Energy Dispersive X-Ray (EDX), X-ray photoelectron (XPS) and Raman spectroscopy studies, indicating that FLG is mainly deposited on the surface wrapping the TiO₂ nanoparticles. The presence of FLG in low concentrations and the mechanochemical activation are the key steps to improve the photocatalytic activity of TiO₂ nanoparticles on these hybrid nanocomposites. The TiO₂-FLG-0.5% hybrid nanocomposite, with circa 1.9 % content of graphitic carbon in surface, has showed the best photocatalytic performance in the degradation of pesticides. Pesticides were completely removed at 350 minutes, and around 82 % of total organic carbon (TOC) conversion was achieved at 540 minutes of irradiation time.

Keywords

Graphene, TiO₂, nanoparticles, environmental, pesticides

1. Introduction

Nowadays, the employment of pesticides is still growing principally due to their use in the agricultural sector [1]. Despite their benefits for both control pests of public health concern and product storage-related applications, they provoke lasting detrimental effects on water quality. The wide extent of pesticides applied to farming awakes controversial because of the severe cumulative environmental damages [2], concluding that regulation and controls are required.

The mixing of otherwise clean water bodies with water used for irrigation in fields also leads to contamination as the latter is likely to contain large amounts of fertilizers, pesticides, and herbicides, several of which have negative effects on humans and animals when consumed. In this context, among the principal disadvantages of pesticides compounds can be emphasized their variety, toxicity and high accumulation as persistent organic pollutants (POPs) in water and in the ambient due to their infiltration into surface, groundwater, soil, and their capacity to volatilize [3-5].

Particularly, recalcitrant pesticides are not effortlessly and straightforwardly eliminated, as a consequence of they are non-biodegradable pollutants. For this reason, nowadays the development of efficient technologies for removing these types of POPs (i.e. pesticides) from natural resources, including water treatment is still a great concern. [1]

In the last decades, European Union (EU) has constantly adapted the legislation to guard and recover the quality of polluted water resources. Newly, the EU [6] has established the main requisites, of mandatory compliance, with respect to agricultural exploitations with high harmful pesticides pollution, with the aim to reduce their emissions and the generated wastes.

In order to develop efficient wastewater treatments for pesticides removal, avoid bio-recalcitrant organics intermediates and diminish their accumulation, important efforts are being carried out.

Among the different conventional wastewater processes, biological treatments have limited success in this case. The high toxicity of pesticides for microorganisms reduces their final efficiency, remaining as persistent contaminants in water streams.

On the other hand, the water-soluble pesticides (isoproturon, alachlor, methomyl and pyrimethanil) studied in this work are considered among priority substances, are included in the European Water Framework Directive Directive 2013/39/EU; and classified in the Watch List of Decision 2015/495/EU. [7]

The concentrations in real wastewater could be lower, but in agriculture industrial installations, where products are washed up and conditioned, the concentration of pesticides could reach even higher concentrations. Moreover, in order to obtain reliable Liquid Chromatography (HPLC) and Ionic Chromatography (IC) analytical results lesser pesticides concentration could drive to important errors, difficult to interpret.

In this context, the application of an advanced oxidation processes (AOPs) as pre-treatments of these toxic pesticides could generate more readily biodegradable organic intermediates and drive to a viable and effective option to treat pesticides contaminated wastewater. [8] These AOPs are managed to oxidize unselectively a wide range of organic chemicals with excellent removal efficiency.[9] AOPs are based on generation of strong oxidants, mainly based on the powerful oxidation capacity of OH-radicals ($\bullet\text{OH}$) [10]. Currently, photocatalysis is one of the most promising AOPs approach to transform recalcitrant pollutants into harmless substances [11] in an environmental-friendly way due to low production costs, mild ambient conditions, rapid degradation of pollutants without the generation of sludge, strong oxidizing power under ultraviolet irradiation,[1] and the possibility of being applied in aqueous environments by utilizing solar energy.[12]

In this context, heterogeneous solar photocatalysis is a clear example of the successful use of solid catalysts in the degradation and mineralization of a wide range of organic pollutants, such as pesticides or herbicides from agricultural industry [13, 14]; resulting the complete oxidation to CO_2 and H_2O , where the energy needed to photo-excite the catalyst can be directly obtained from the sun. [15] Heterogeneous photocatalysis is based on the excitation of a solid-catalyst, usually a semiconductor, by absorbing radiation of different wavelengths.[16] One of the most attractive and efficient semiconductor photocatalyst is TiO_2 , [17] that in spite of its high versatility, presents some significant disadvantages such as low photocatalytic efficiency (high rate of electron/hole pair recombination [18]), activation in UV region (3.2 eV bandgap energy for anatase [19, 20], therefore a radiation with wavelength $<387\text{nm}$ is required [20, 21]) which means $<5\%$ of the solar light [22, 23]). TiO_2 exists in three different crystalline phases: rutile (tetragonal, thermodynamically stable form in bulk), anatase (tetragonal, thermodynamically metastable) and brookite

(orthorhombic, thermodynamically metastable). [24] Many strategies has been developed to improve the photocatalytic performance of TiO₂ (enhancing the visible light absorption and through the reduction of fast electron–hole recombination) including doping with non-metallic particles, noble metals or transition metal elements, [25-27] adding an adsorbent,[28, 29] and through the heterojunctions with other materials, such as graphene, [25] to improve the separation between free carriers. [30-37] Due to their interesting properties, various 2D nanomaterials have been used in the treatment and degradation of pesticides demonstrating promising results in this area. [38]

Graphene is a one-atom-thick monolayer of carbon atoms packed in a two-dimensional honeycomb lattice, which has interesting physical, chemical, electronic, thermal, and mechanical properties,[39] high charge carrier mobility,[40, 41] specific surface area ($\sim 2600 \text{ m}^2\text{g}^{-1}$),[42] and adsorption capacity [43]. Graphene can serve as an excellent photodetector in a range of lengths much larger than conventional detectors due to their wavelength independence[44] and ultrafast response as result to their high mobility. All these excellent properties make graphene a good candidate in applications in solar cells and photoactive catalysts,[44] being an excellent material in the synthesis of new hybrid structures to improve the performance of TiO₂ base photocatalysts.[45-49] Graphene enhances the photocatalytic efficiency of TiO₂,[50-52] due to many factors such as large surface area, which supports highly disperse TiO₂ nanoparticles photocatalyst and stabilizes charge separation (trapping electrons from TiO₂),[53] it solves the problem of large bandgap energy[54] and, reduces the recombination by Schottky barrier of photogenerated electron-hole pairs.[55-57]

Hybrids graphene/TiO₂ have been extensively studied[58, 59] mainly for applications like lithium-ion batteries[60] to improve performance in photocatalytic applications[61] catalysis,[62] solar cells,[63] and CO₂ reduction. [64],[65] The preparation of most of hybrid graphene-TiO₂ photocatalysts developed and studied in the scientific literature to date, ranging from simple physical mixing with or without sonication of both materials [66], in situ growth of graphene on the TiO₂ particles themselves, its synthesis through sol-gel processes [67], liquid phase deposition [68], aerosol [69], chemical vapour deposition[70], spin coating [71], etc. [72], to preparation methods based on hydrothermal or solvothermal synthesis to obtain generally hybrid systems based on TiO₂ and graphite oxides (GO) or reduced graphite oxides (rGO) [73]; where the reduction of graphite oxide can be carried out by physical procedures, traditional redox reagents or chemical agents from graphite, with the consequent generation of highly toxic acidic residues.

Therefore, different strategies are currently being implemented to achieve new optimized titanium-graphene nanocomposites. On the one hand, by means of new safer, more ecological and less waste-generating graphene syntheses using natural or biocompatible reducing agents; and, on the other hand, to improve the interaction and formation of Ti-C and/or Ti-O-C bonds between TiO₂ and own graphene, and thus achieve a good hybrid graphene-TiO₂ photocatalyst. In order to improve this interaction, new developments have been designed in recent years that use different organic molecules or polymers to functionalize graphene and facilitate the anchoring of TiO₂ nanoparticles, leading to more efficient and durable photocatalyst compounds [74] [75].

Consequently, in this work a process to prepare few layers graphene (FLG), from the exfoliation of graphite using melamine as exfoliant agent, through a mechanochemical treatment, according to a protocol previously published [76, 77], was used to directly get the starting graphene material. The great novelty of this work has consisted in developing a procedure for the synthesis of TiO₂-FLG hybrid nanocomposites, based on the union of titanium oxide directly with graphene, from a preparation methodology by means of mechanochemical synthesis.

Unlike other syntheses of this type of hybrid photocatalysts, where graphene oxide (GO) or even reduced graphene oxide (rGO) previous step is required, in this case, graphite oxidation step to produce GO was omitted. Consequently, the consumption of large quantities of corrosive and harmful pollutants reagents were avoided. Analogously, additional time-lasting classic steps of catalysts synthesis methodologies, such as sol-gel, hydrothermal, etc., or even physical mixtures of both materials were not employed [66] . The proffered methodology starts directly from FLG and the TiO₂ nanoparticles prepared through an innovative, totally sustainable, and ecological procedure. The final titania-graphene nanocomposite (TiO₂-FLG) was obtained in a unique step with the only use of a planetary ball mill. In this type of mechanochemical synthesis with high energy impulses, a mechanical activation takes place, similar to the case of a conventional physical mixture; but, in addition, alterations in the structure of the material and its chemical composition are achieved. Since it is a reactive synthesis process which induces the generation of chemical reactions in a solid state at room temperature, results in a much more sustainable and ecological procedure than the traditional synthesis methods.

The mechanochemical synthesis of mixed materials from reactive ball milling is almost an ideal method to prepare nanocomposites not only because of its simplicity, but mainly because of the possibility of forming

a nanocomposite characterized by a uniform distribution of particle sizes at room temperature, generating unique phases and crystalline microstructures [78, 79]. In addition, an *in-situ* synthesis route results in the production of materials with greater homogeneity in their microstructure and greater thermodynamic stability than those synthesized from conventional ex situ methodologies [80].

In this context, the main goal of this work has consisted of optimizing a synthesis methodology based on mechanochemical treatment in a planetary mill to get hybrid TiO₂-FLG nanocomposites for their application in the photocatalytic degradation of a complex mix of pesticides, classified by EU as priority pollutants (isoproturon, alachlor, methomyl and pyrimethanil). The effect of FLG loading in the hybrid photocatalysts was analyzed to define an optimal ratio of FLG to TiO₂ and compared to physical mixtures of TiO₂+FLG to discriminate the existence of a synergic effect in the photocatalytic process studied.

2. Material and methods

2.1 Photocatalysts Synthesis

2.1.1 Mechanochemical production of Few-Layer Graphene (FLG).

Few-Layer Graphene (FLG) was synthesized by exfoliation of graphite using melamine as exfoliating agent through a green mechanochemical treatment as previously published protocol.[76]

2.1.2 Synthesis of TiO₂ nanoparticles.

In an Erlenmeyer, 100 mL of Ethanol and 400 μ L of KCl (0.01M-pH 8.5) were added with stirring at 1200 rpm, after that 4.4 mL of Ti precursor (titanium isopropoxide) were poured. When a white precipitation was observed the stirring was decreased at 150 rpm (approx. 1 min) for 6 hours and the Erlenmeyer was covered by Parafilm®, followed for further dialysis (7 changes each 2 hours). After that, the TiO₂ was lyophilized for 2 days at -80°C at a pressure of 0.005 bar.

2.1.3 Mechanochemical synthesis of Few Layer Graphene (FLG) decorated with TiO₂ nanoparticles-Hybrid nanocomposites.

All hybrid photocatalysts were prepared as following: FLG was mixed with pre-synthesized TiO₂ NPs with a proportion of FLG from 0.1 to 1 wt. % in a Retsch PM100 planetary mill at 30 min and 100 rpm in zirconium grinding bowl of 250 mL with 15 zirconium balls (1 cm diameter) in air atmosphere. The resulting solid mixtures were dispersed in 100 mL water for further lyophilization for 72 hours at -80°C and pressure

of 0.005 bar. The hybrid nanocomposites are nominated as TiO₂-FLG X %, where X corresponds to FLG percentage added in the synthesis procedure, in wt. %.

2.1.4 Physical mixtures of Few Layer Graphene plus TiO₂ nanoparticles

Two different photocatalysts based on physical mixtures of FLG and TiO₂ nanoparticles have been prepared through mortar and sonication of both materials.

TiO₂+FLG 0.5 %-sonicated catalyst was obtained by mixing 300 mg TiO₂ NPs, 1.5 mg FLG, and 100 mL of water. This solution was ultrasonicated during 30 min, following by lyophilization at the same conditions explained above.

Finally, 1.5 mg of FLG and 300mg of TiO₂ nanoparticles were mixed manually in an agate mortar (80 mm in diameter and 30 mL) with pestle for 30 minutes. After this treatment, the obtained powder was dispersed in 100 mL water for further lyophilization of the mix at the same conditions mentioned above to obtain the physical mixture called TiO₂+FLG 0.5 %-mortar.

2.2 Characterization techniques

XRD data were recorded on a Philips (Panalytical) model X'Pert MPD diffractometer using Cu K α 1 (0.154056 nm) at 40 kV and 40 mA. Diffraction patterns were collected over a range of 5–60° 2 θ at a scan rate of 0.01° 2 θ min⁻¹ and a scan velocity of 0.004°s⁻¹. The crystallite size, d , was calculated according to the Scherrer equation:

$$d = \frac{0.9 \cdot \lambda}{2B \cdot \cos \theta}$$

where B is the corrected peak width, $\lambda = 0.154$ nm, and θ is the reflection angle, in this case, the plane (101) of anatase was used.[81]

Raman spectra were recorded on an InVia Renishaw microspectrometer equipped with a 532 nm point-based laser. In all cases, power density was kept below 1 mW· μ m⁻² to avoid laser heating effects. Raman analyses were performed in the solid-state under ambient conditions. The resulting spectra (after at least 30-40 random locations on each sample) were fitted with Lorentzian-shaped bands in their D, G, and 2D peaks to ascertain band positions, widths, and intensities.

UV-Vis diffuse reflectance spectra of the powder photocatalysts were registered in a Cary 5000 Agilent spectrometer equipped with an integrating sphere (using Spectralon® PTFE as internal reference).

Thermogravimetric analyses (TGA) were performed with a TGA Q50 (TA Instruments) at $10\text{ }^{\circ}\text{C}\cdot\text{min}^{-1}$ under nitrogen flow, from $100\text{ }^{\circ}\text{C}$ to $800\text{ }^{\circ}\text{C}$.

The energy of the nanocomposite band gap was determined by Tauc plots of Kubelck-Munk function from UV-Vis Diffuse Reflectance spectroscopy data,[82] considering an indirect allowed transition. [83]

Transmission Electron Microscopy (TEM) analyses were performed on stable dispersions of graphene (the same used for Raman analysis) diluted as necessary and dip-casted on Lacey copper grids (3.00 mm, 200 mesh), coated with carbon film and dried under vacuum. The samples were investigated using a High-Resolution Transmission Electron Microscope (HRTEM) JEOL 2100 at an accelerating voltage of 100 kV. Scanning Electron Microscopy (SEM) images, elemental mapping and EDX analyses were performed in a GeminiSEM 500 field emission instrument (Zeiss). SEM images were acquired on the same lacey copper grids used in TEM analyses. Meanwhile, EDX analyses and elemental mapping were measured in pellets of the different nanocomposites. These pellets were made compressing each nanomaterial until obtaining a flat dense surface to analyze. EDX relationship were calculate dividing the percentage of C and O between the quantity obtained of Ti, only these three elements were presented in the samples.

XPS was registered with a K-Alpha Thermo Scientific spectrometer in order to obtain qualitative information about surface composition and atomic oxidation state. EDX with Microanalysis of Energy Dispersive Spectroscopy (EDS) and Electron Backscatter Diffraction (EBSD) (both of them OXFORD with advanced packages) were employed to know quantitatively the surface composition, respectively; afterwards, the corresponding XPS and EDX atomic ratios were calculated.

2.3 Photocatalytic activity

Photocatalytic runs were carried out in a semi-continuous slurry type photoreactor, previously described, [84] surrounded by 10 fluorescent lamps: 6 UV lamps (Narva LT 15W/073 Black-Light Blue, $\lambda_{\text{max}} = 366\text{ nm}$) and 4 Vis lamps (Narva LT 15W/865 Cool Day-Light, $\lambda = 400\text{-}780\text{ nm}$) with a total irradiance of $40\text{ W}\cdot\text{m}^{-2}$ (measured with a Kipp & Zonen model CUV-4 broadband UV radiometer; 306-383 nm).

The mixture of pesticides consisted of: $[\text{isoproturon}]_0 = [\text{alachlor}]_0 = [\text{methomyl}]_0 = [\text{pyrimethanil}]_0 = 5.0\text{ mg}\cdot\text{L}^{-1}$. The solution containing the mixture of these pollutants at natural pH, was premixed with $200\text{ mg}\cdot\text{L}^{-1}$ of each photocatalyst, in dark conditions, for 30 min to guarantee homogeneous mixing in the photoreactor as well as the adsorption equilibrium of the pollutants on the photocatalysts. After that,

photocatalytic runs (using $75 \text{ N cm}^3 \cdot \text{min}^{-1}$ of oxygen flow) started by turning on all the lamps, and samples were withdrawn at selected periods to follow the reaction.

Azura Plus, Knauer High Performance Liquid Chromatography, HPLC, with Diode-Array detection was used to identify and quantify the pesticides after filtration of samples with $0.22 \mu\text{m}$ size hydrophilic PTFE filters. Calibration curves for each pesticide was previously constructed in identical analytical conditions within the analysis range. An Ultrasep ES PEST $5 \mu\text{m}$ (Dr. Maisch) column ($250 \times 3 \text{ mm}$) was used as stationary phase. The mobile phase was composed by ACN/acidic water (0.1% phosphoric acid) in gradient mode, at $0.8 \text{ mL} \cdot \text{min}^{-1}$ flow rate.

Short-chain organic acids and inorganic ions were also analyzed by an ion chromatograph with chemical suppression (Metrohm 883 Basic IC Plus) and a conductivity detector using a Metrosep A supp 7 column (250 mm length, 4 mm diameter) as stationary phase for anions and Metrosep C 6 in the case of cations; 3.6 mmol/L sodium carbonate and $1,7 \text{ mmol} \cdot \text{L}^{-1}$ nitric acid/ $1,7 \text{ mmol} \cdot \text{L}^{-1}$ dipicolinic acid, were the mobile phases, respectively. The total organic carbon content was determined in an infrared-detector TOC-VCSH/CSN Shimadzu analyzer.

3. Results and Discussion

The synthesized TiO_2 -FLG hybrid nanocomposites have been characterized by different physico-chemical techniques such as XRD, SEM, TGA, HRTEM, Raman and UV-Vis spectroscopy, to determinate their main properties, analyzing the interactions between TiO_2 nanoparticles and FLG. The XRD patterns (see **Figure S.1**) revealed that all these nanocomposites presented the same crystal structure, with anatase as the main crystalline phase ($\sim 97.5 \%$) and brookite as secondary phase ($\sim 2.5 \%$). Similar anatase and brookite sizes were observed when FLG was introduced into the hybrid nanocomposite, with mean crystallite sizes close to 5 nm (see **Table S.1**). Regarding electronic properties, almost no differences were observed when the FLG content was increased (3.07 - 3.14 eV).

On the other hand, from Raman Spectroscopy (see **Figures 1 and Table S.2**) anatase phase exhibited four Raman active modes: two E_g (151 and 633 cm^{-1}), one B_{1g} (409 cm^{-1}), and one A_{1g} (515 cm^{-1}),^[85] where the peak position and broadening of the low-wavenumber E_g mode in anatase nanocrystals have commonly been explained through factors such as phonon confinement, thermal effects, and crystal defects.^[24, 86] These Raman active modes are showed in **Figure 1a** for all the FLG- TiO_2 hybrid nanocomposites together with

the D, G, and 2D bands from graphene that were revealed at $\sim 1350\text{ cm}^{-1}$, $\sim 1580\text{ cm}^{-1}$, and 2700 cm^{-1} . The D band (sp^3 bonds) is due to the disorder or defects in the graphene structure and G band (sp^2 bonds) arises from the stretching of the C-C bond in graphene. Meanwhile, the 2D band is interrelated to the band structure of graphene layers.[87] All the different parameters are showed in **Table S.2**. The relationship between the D and G band are 0.46, 1.34, 1.08, 0.84, 0.51 for FLG, TiO_2 -FLG 0.10%, TiO_2 -FLG 0.25%, TiO_2 -FLG 0.50% and TiO_2 -FLG 1.0%, respectively. This increment is due to the defects in graphene layers by the anchorage of TiO_2 nanoparticles in their structure.

Although no significant changes have been observed by XRD, interesting differences were observed by Raman. The E_g mode (see **Figure 1b**) was the most intense band of anatase and is commonly used for analysis [88]. The asymmetric and broadening shape of the E_g modes was evident for TiO_2 -FLG 0.0%, TiO_2 -FLG 0.1% and TiO_2 -FLG 0.25%, which can be contributed to a phonon-confinement due to small grain sizes [89]. Whereas TiO_2 -FLG 0.5% and TiO_2 -FLG 1.0% showed larger and more symmetric peaks indicative of higher crystalline domains, principally in the TiO_2 -FLG 0.5% nanocomposite. In general, all these hybrid photocatalysts have shown a blue shift in E_g and B_{1g} the bands (151 cm^{-1} and 409 cm^{-1}), in comparison with

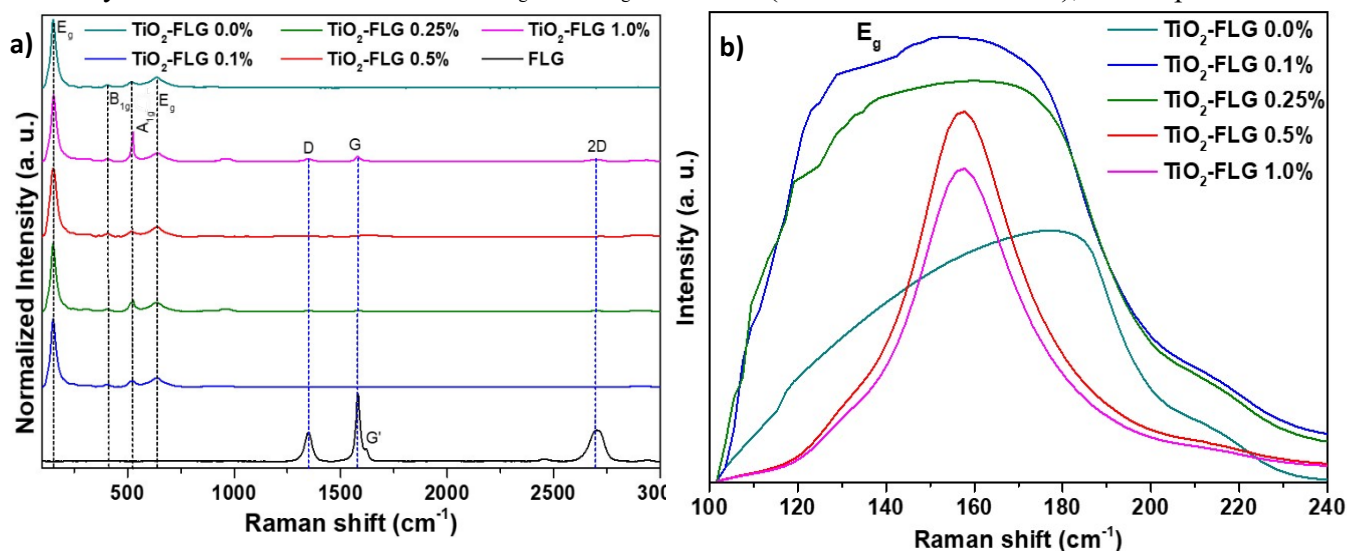


Figure 1. Raman spectroscopy of a) the TiO_2 -FLG hybrid nanocomposites and b) the E_g band of TiO_2 -FLG hybrid nanocomposites.

the TiO_2 -FLG 0.0% and a red shift in the G band of graphene.

TiO_2 -FLG 0.50% hybrid nanocomposite showed the lowest shift change in the E_g and B_{1g} , which is in agreement with a larger crystalline domain and the higher shift in the G band, being able to associate to hole doping in the nanocomposite.[90] There is a correlation between the intensity of the D, G and 2D band and the concentration of FLG in all the different hybrid nanocomposites. Moreover, it was possible to observe a

slight shift in the 2D and G peaks from 5 to 8 cm^{-1} for all the different nanocomposites, which implies an interaction between the graphene structure and the TiO_2 nanoparticles. So, a direct correlation between the quantity of FLG in the nanocomposites and the relation between the intensity of the E_g from TiO_2 nanoparticle at 639 cm^{-1} and the intensity of 2D band of FLG at 2700 cm^{-1} was evidenced, which decreases with the amount of graphene. TGA analysis in air atmosphere (see **Figure S.2 and Table S.3**) was employed to characterize the thermal stability of these hybrid nanocomposites. It was possible to observe weight losses in the range between $200\text{-}350^\circ\text{C}$, for as-synthesized TiO_2 nanoparticles and for all the different hybrid nanocomposites. These weight losses below 200°C corresponded to the removal of physically adsorbed water, meanwhile, those above 200°C corresponded to loss of surface $-\text{OH}$ groups in the form of water and production of new $\text{Ti}-\text{O}-\text{Ti}$ bonds [91]. TGA analysis in nitrogen atmosphere was also used to characterize all these nanocomposites. A high thermal stability was observed under these conditions due not only to the stability of TiO_2 nanoparticles but also to the stability of FLG which did not present oxidative defects (see **Figure S.3 and Table S.4**).

Atomic composition obtained from XPS and EDX, in %, and the corresponding O/Ti atomic ratios are shown in **Table 1**. The data obtained from XPS are distorted by the high contamination in carbon compounds found on the surface of the photocatalysts particles, so it was not possible to draw reliable conclusions from these results. However, the results obtained from EDX followed a logical progression. As the amount of FLG increased, the proportion of titanium and oxygen decreased, and the proportion of carbon increased.

Table 1. Atomic composition and O/Ti ratios of TiO_2 -FLG hybrid nanocomposites and TiO_2 +FLG 0.5 % physical mixtures, respectively measured by XPS and EDX.

Nanocomposites	XPS (%)			EDX (%)			(O/Ti) ratios	
	Ti	O	C	Ti	O	C	EDX	XPS
TiO₂-FLG 0.0 %	22.00	54.21	23.79	32.33	67.67	0.00	0.70	0.82
TiO₂-FLG 0.10 %	19.83	54.77	25.40	30.24	64.76	5.00	0.72	0.92
TiO₂-FLG 0.25 %	20.93	55.47	23.61	30.22	64.14	5.63	0.71	0.89
TiO₂-FLG 0.50 %	20.93	55.47	23.61	29.56	64.04	6.40	0.72	0.89
TiO₂-FLG 1.0 %	21.84	55.17	22.99	29.67	62.37	7.96	0.70	0.84

TiO₂+FLG 0.5 % - Mortar	20.37	52.75	26.88	30.30	63.25	6.45	0.70	0.87
TiO₂+FLG 0.5 % - Sonicated	20.46	54.44	25.10	28.41	65.68	5.92	0.77	0.89

The proportion of carbon is high, if the amount added in the synthesis is considered, which indicated that FLG is mainly deposited on the surface of the TiO₂ nanoparticles, and the preparation method does not seem to be relevant in terms of composition. Finally, from a comparative analysis of O/Ti atomic ratios obtained from EDX and XPS, respectively, it can be observed that both O/Ti ratios were not dependent on FLG loading in these hybrid nanocomposites and it must be linked to TiO₂ fraction.

The Ti 2p spectrum showed two peaks at approximately 458.8 eV (Ti 2p_{3/2}) and 464.4 eV (Ti 2p_{1/2}), which are typical of TiO₂ (see **Figures S.4**). The O 1s spectrum also showed two peaks. The one with highest intensity was near 530 eV which is typical of metal oxides, so it can be assigned to TiO₂. The second, approximately at 531.5 eV is due to oxygenated organic functional groups. It was not possible to discern whether they belong to FLG molecules that may have been oxidized or to the contamination of organic compounds that were mentioned above.

However, although C 1s spectrum resulted difficult to interpret because of the high carbon surface contamination, it was possible to observe in the deconvolution of this peak that a component appeared at energies close to 284 eV that was not observed in the sample without FLG. Results of deconvolution are shown in **Table 2**.

Table 2. Deconvolution of C 1s XPS spectra.

Nanocomposites	Peak 1		Peak 2		Peak 3		Peak 4	
	B. E. (eV)	%	B. E. (eV)	%	B. E. (eV)	%	B. E. (eV)	%
TiO₂-FLG 0.0 %	283.88	0.23	284.76	70.11	286.08	21.48	288.61	8.18
TiO₂-FLG 0.10 %	283.96	6.36	285.09	64.52	286.28	23.09	289.04	6.04
TiO₂-FLG 0.25 %	284.06	6.70	285.01	66.96	286.24	20.04	288.92	6.30
TiO₂-FLG 0.50 %	283.95	7.85	285.04	70.45	285.99	16.32	288.97	5.38
TiO₂-FLG 1.0 %	283.97	9.67	285.08	62.48	286.34	20.15	288.96	7.70
TiO₂+FLG 0.5 % - Mortar	283.89	12.01	284.99	67.19	286.00	15.94	288.95	4.86
TiO₂+FLG 0.5 % - Sonicated	283.77	6.43	285.00	84.27	286.34	6.77	288.85	2.52

***B. E. (Binding Energy)**

The intensities of peaks 2, 3 and 4 varied somewhat randomly, so they can be assigned to light, medium or heavily oxidized structures of the contaminating organic matter, respectively. However, peak 1 intensity increased, in general, with the amount of FLG added, from practically 0 to 9.67 %. The low value of the bonding energy also makes it possible to state that this component is due to the presence of graphene. XPS C1s deconvolution peaks of TiO₂-FLG 0.0%, TiO₂-FLG 0.5% and TiO₂-FLG 1.0% nanocomposites, respectively, were shown in **Figure S.5**, where it can be seen that, with a very tight deconvolution, in the nanocomposite containing only TiO₂ there is hardly any component of peak 1.

HRTEM and SEM images (see **Figure 2**) showed the uniform distribution of the TiO₂ nanoparticles on the sample and the crystalline phase of anatase corresponding with the plane (101) (see **Figure S.1**). The distribution size of the most representative nanocomposite TiO₂-FLG 0.5 % was showed in the **Figure S.6** with an average diameter of 9.2 ± 5.1 nm of TiO₂ nanoparticles.

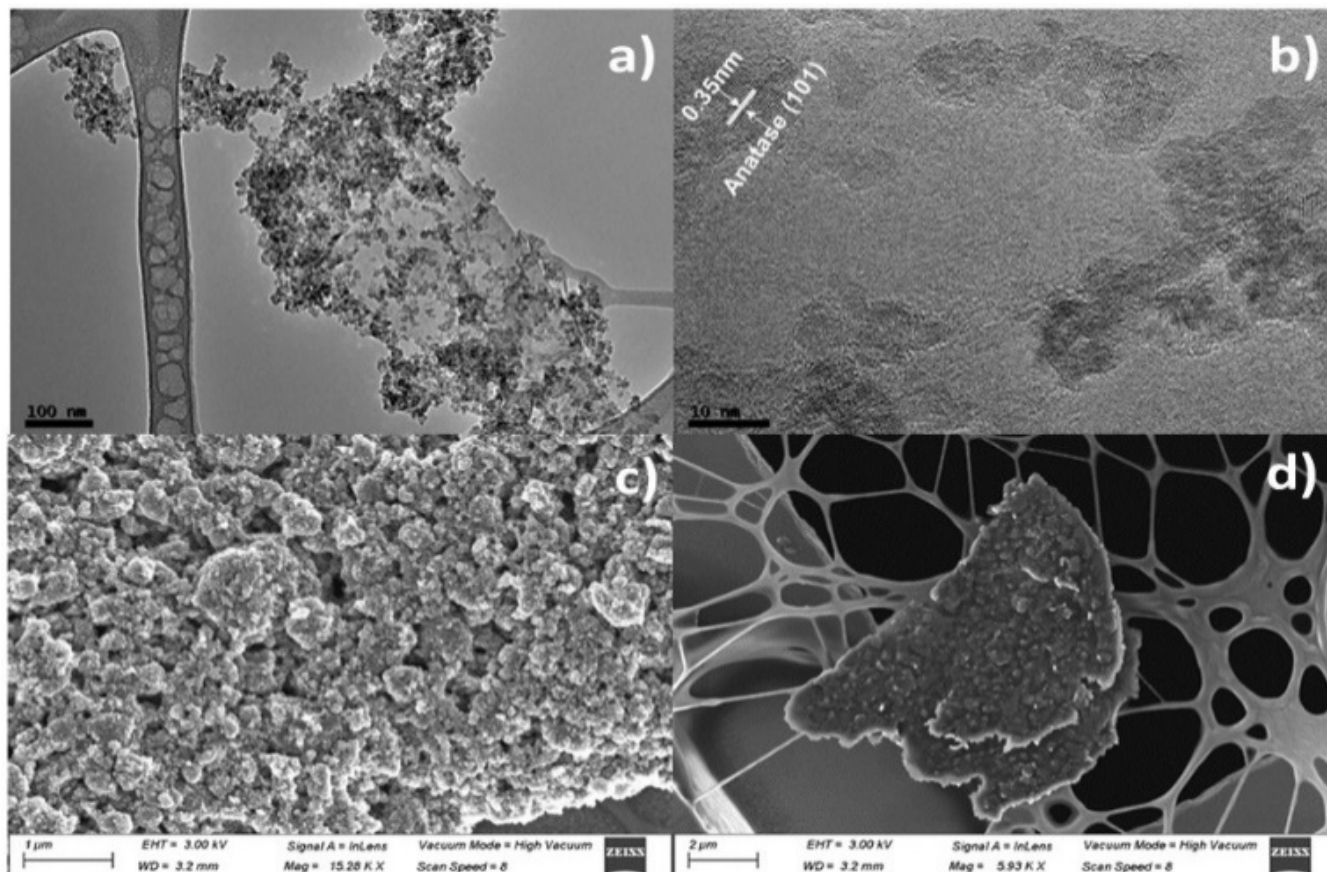


Figure 2. Representative images of TiO₂-FLG 0.5 % hybrid nanocomposite

The distribution of FLG on the different nanocomposites was analyzed using elemental mapping (see **Figures S.7** showing same areas analyzed by EDX in **Table 1**); C, Ti, and O are the elements found in the nanocomposite mapping. The proportion of titanium is very similar in all nanocomposites, with a slight increment in the carbon presence at 0.25, 0.5 and 1%.

A comparative study of the photodegradation of a selected mixture of pesticides was carried out to select the optimal FLG content in the TiO₂-FLG hybrid nanocomposite, where low concentrations of graphene were mainly used in aqueous photocatalytic applications.[73]

Photolysis runs were performance in absence of photocatalysts, and blank runs were also carried out in dark conditions under the same operating conditions. Negligible degradation was observed in any case (pesticides conversions < 5 % and TOC conversions < 1 %). On the other hand, adsorption equilibrium was

always arisen during dark conditions, given the low FLG contents in the nanocomposite, where even lower pesticides and TOC adsorption conversions were found (< 1%) in all cases.

TiO₂-FLG nanocomposites were investigated in the photocatalytic degradation of the pesticides mix. **Figure 3 and Table 3** show the effect of FLG loading on TOC conversions. It can be observed that the photo-oxidation of pesticides was improved with loading as low as 0.1 wt. % of FLG (TiO₂-FLG 0.1 %). However, the higher pesticides and TOC conversions were obtained by increasing the FLG content up to 0.5 wt. % (TiO₂-FLG 0.5 %). Though, with a higher FLG content, such as 1 wt. % (TiO₂-FLG 1.0 %), lower pesticides and TOC conversions were obtained, probably as a consequence of the poor radiation rate reaching titania nanoparticles, as prior deduced from XPS analysis FLG seems to wrap titania nanoparticles.

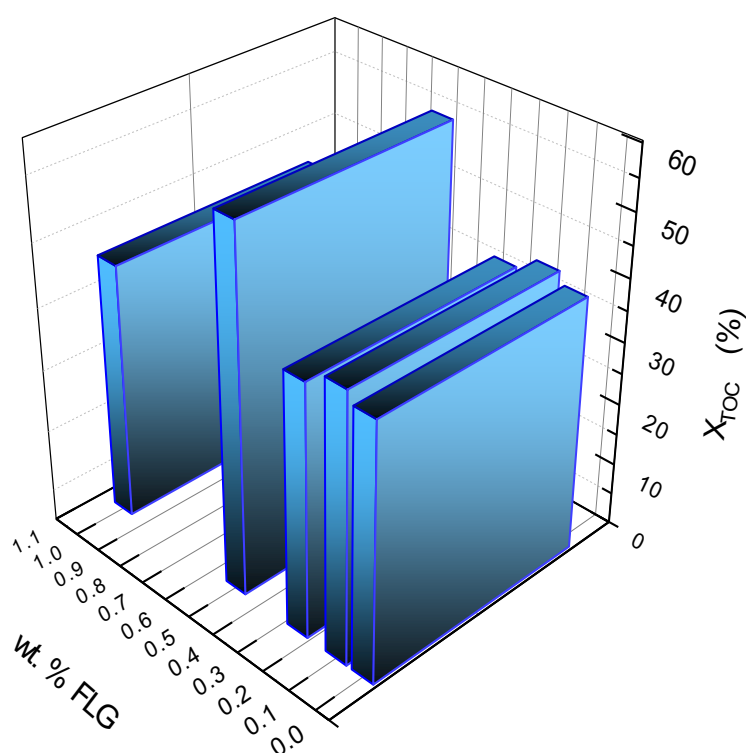


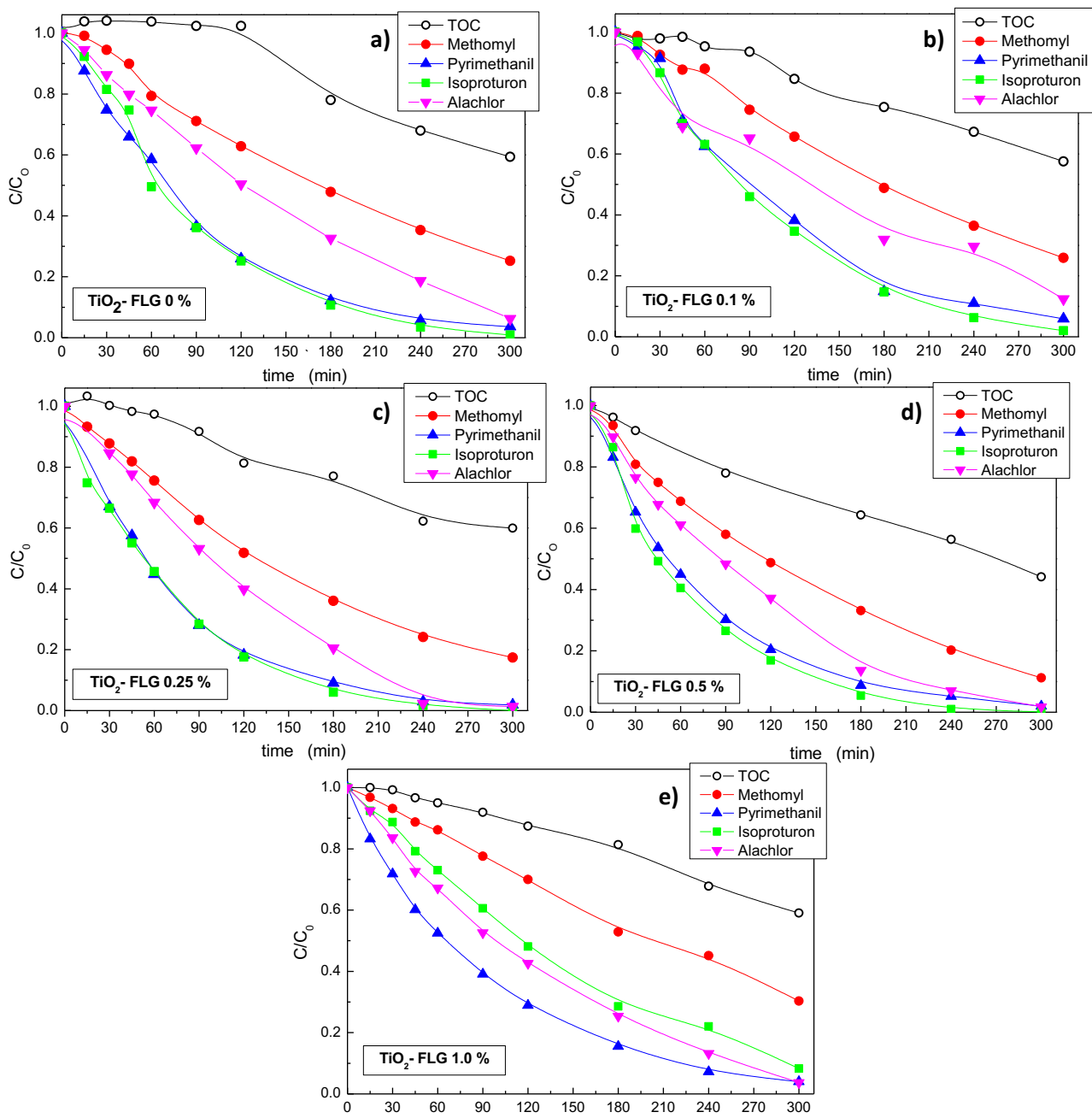
Figure 3. Effect of percentage of FLG on photocatalytic performance at 300 minutes of irradiation time with the TiO₂-FLG hybrid nanocomposites.

Table 3. Pesticides and TOC conversions after 300 minutes of irradiation time of TiO₂-FLG nanocomposites and TiO₂+FLG 0.5 % physical mixtures.

Nanocomposites	(%)				
	X _{Isoproturon}	X _{Alachlor}	X _{Methomyl}	X _{Pyrimethanil}	X _{TOC}
TiO₂-FLG 0.0 %	99.7 ± 0.05	93.8 ± 0.07	74.8 ± 0.08	96.4 ± 0.01	40.9 ± 0.03
TiO₂-FLG 0.10 %	94.1 ± 0.03	87.6 ± 0.06	74.1 ± 0.09	98.0 ± 0.02	42.4 ± 0.01
TiO₂-FLG 0.25 %	98.1 ± 0.06	98.7 ± 0.05	82.6 ± 0.03	100 ± 0.00	40.8 ± 0.02
TiO₂-FLG 0.50 %	99.9 ± 0.01	98.2 ± 0.02	88.8 ± 0.01	100 ± 0.00	57.5 ± 0.01
TiO₂-FLG 1.0 %	91.7 ± 0.02	96.3 ± 0.03	85.8 ± 0.02	97.9 ± 0.03	40.6 ± 0.04
TiO₂+FLG 0.50 % - Mortar	87.7 ± 0.03	85.9 ± 0.02	65.8 ± 0.03	90.6 ± 0.03	36.9 ± 0.04
TiO₂+FLG 0.50 % - Sonicated	91.4 ± 0.02	88.8 ± 0.01	76.0 ± 0.04	94.8 ± 0.01	46.7 ± 0.01

Although almost all the pesticides were removed after 300 minutes of irradiation time, a TOC concentration was still found at the end of the process, as it can be seen in the evolution of pesticides and TOC for all the studied TiO₂-FLG hybrid nanocomposites (see **Figures 4**). Whereas complete removal of isoproturon, alachlor, and pyrimethanil were always achieved, small traces of methomyl together with some amounts of oxidation by-products remained after 5 h reaction as it was revealed by the TOC evolution curves. These oxidation products mostly corresponded to some organic by-products and short-organic acids, mainly acetic and formic, responsible for the detected residual organic matter. In all cases, different photodegradation rates were observed for every pesticide in each titania-graphene hybrid nanocomposite, where methomyl has always presented the slowest photodegradation rate.

Most authors agree that the rate of photo-oxidation of organic pollutants with irradiated TiO₂ based photocatalysts roughly follows the Langmuir-Hinshelwood (L-H) law,[15, 92] being also accepted that the corresponding rate constants and orders are only “apparent”. [93]



Figures 4. Evolution of pesticides and TOC along the photocatalytic degradation with the TiO_2 -FLG 0 %, 0.1 %, 0.25 %, 0.5% and 1.0% nanocomposites.

For that reason, overall reaction rate constants are very difficult to calculate since the photocatalytic reactions are not expected to follow a simple kinetic model. The complexity of the results arises because TOC is a sum parameter, often including several by-products, that undergo manifold reactions since hydroxyl radicals react non-selectively, and numerous organic intermediates can be generated along the photocatalytic degradation frequently defined as sequential decarboxylation reaction before achieving complete mineralization to CO₂ and H₂O [94]. Therefore, considering that the photodegradation of the mixture could be suitably fitted to a modified Langmuir-Hinshelwood (L-H) kinetic scheme,[95] the apparent first order-constants values were calculated for each pesticide and shown in **Figure 5**. In addition, the zero order TOC constants (k_{TOC}) were reckoned and reported too, for all TiO₂-FLG hybrid nanocomposites. In all cases, very good fitting parameters (r^2 , with values around 0.999-0.973) were always obtained, demonstrating that the assumed kinetic model could well describe pesticides and TOC removal as pseudo-first order.

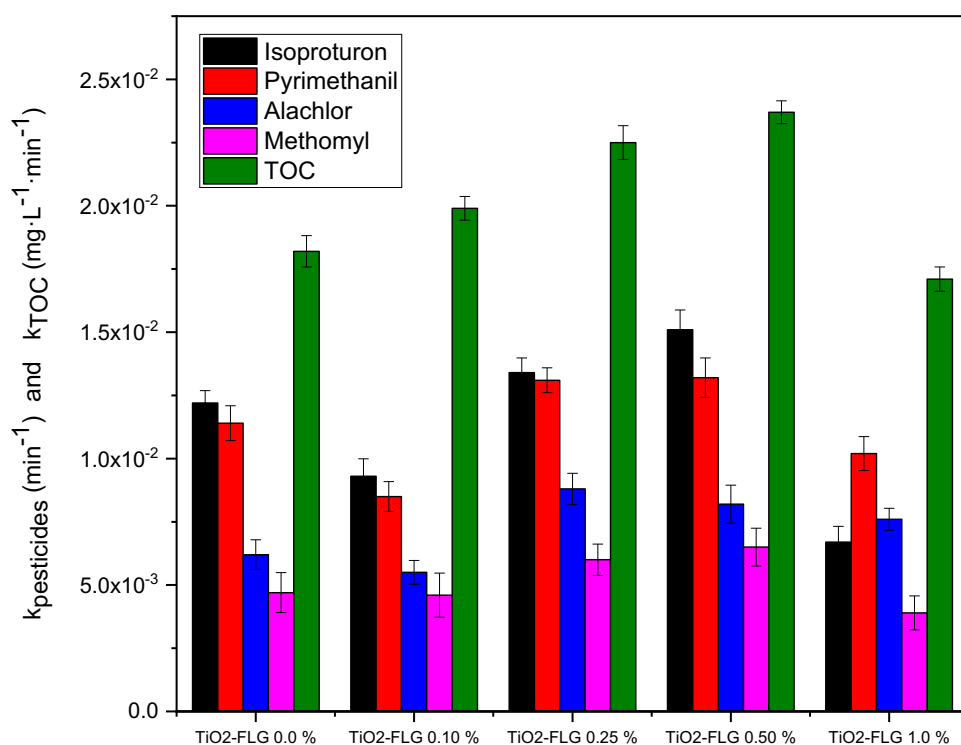


Figure 5. Effect of FLG loading on pesticides and TOC apparent kinetic constants for all TiO₂-FLG hybrid nanocomposites.

The lowest apparent kinetic constants were always found in the case of hybrid nanocomposite with the highest FLG content (TiO₂-FLG 1.0 wt. %), whereas better pseudo-first-order kinetic constants were always observed when FLG content increased up to 0.5 wt. %. Again, the best photodegradation pesticide constants have been achieved with TiO₂-FLG 0.5 wt. %. Same performance evolution was observed in all TiO₂-FLG

hybrid nanocomposites respect to the calculated zero order TOC constants (k_{TOC}), where TiO₂-FLG 0.5 % hybrid nanocomposite exhibited the higher k_{TOC} value as well.

Then, the maximum photoactivity, both in pesticides and TOC conversions at the end of irradiated reaction (300 minutes), was obtained with the 0.5 % wt. FLG loaded nanocomposite. This good behavior may be explained by the pairing synergy balanced between 0.5%FLG and TiO₂, where probably the role played by FLG improved charge separation, driving to long-lasting charges which enhance the final photoefficiency.^{[83,}

^{96]} Therefore, results indicate 0.5 wt. % FLG is the optimal loading in these titania-graphene nanocomposites.

In order to understand the synergic effect between FLG and TiO₂ nanoparticles in the optimal hybrid nanocomposite, two TiO₂+FLG physical mixtures with 0.5 wt. % FLG were prepared by mixing with the corresponding TiO₂ nanoparticles, using mortar and sonication methodologies, TiO₂+FLG 0,5% (mortar) and TiO₂+FLG 0,5% (sonicated), respectively, for comparative purpose. The characterization of these two samples is showed in **Figures S.8-S.110**. XRD revealed the same crystallinity of the previous hybrid nanocomposites, with anatase as main crystalline phase and brookite as secondary phase (see **Figure S.8**). Raman spectroscopy (**Figure S.9a**) showed the same active modes of anatase E_g (151 and 633 cm⁻¹), one B_{1g} (409 cm⁻¹), and one A_{1g} (515 cm⁻¹), and the D, G and 2D band presented in the FLG. In **Figure S.9b** is possible to observe the highest intensity symmetric E_g band in the nanocomposite TiO₂-FLG 0.5%, followed by TiO₂+FLG 0.5% mortar and TiO₂+FLG 0.5% sonicated, which implies a higher crystalline domain size in the hybrid nanocomposite TiO₂-FLG 0.5%. Finally, EDX mapping (**Figure S.10**) of these two-physical mixed photocatalysts has revealed a similar correlation between the quantity of Ti and C in these mixed photocatalyst and the hybrid nanocomposites prepared by ball milling. Despite, some higher aggregates size of FLG were observed.

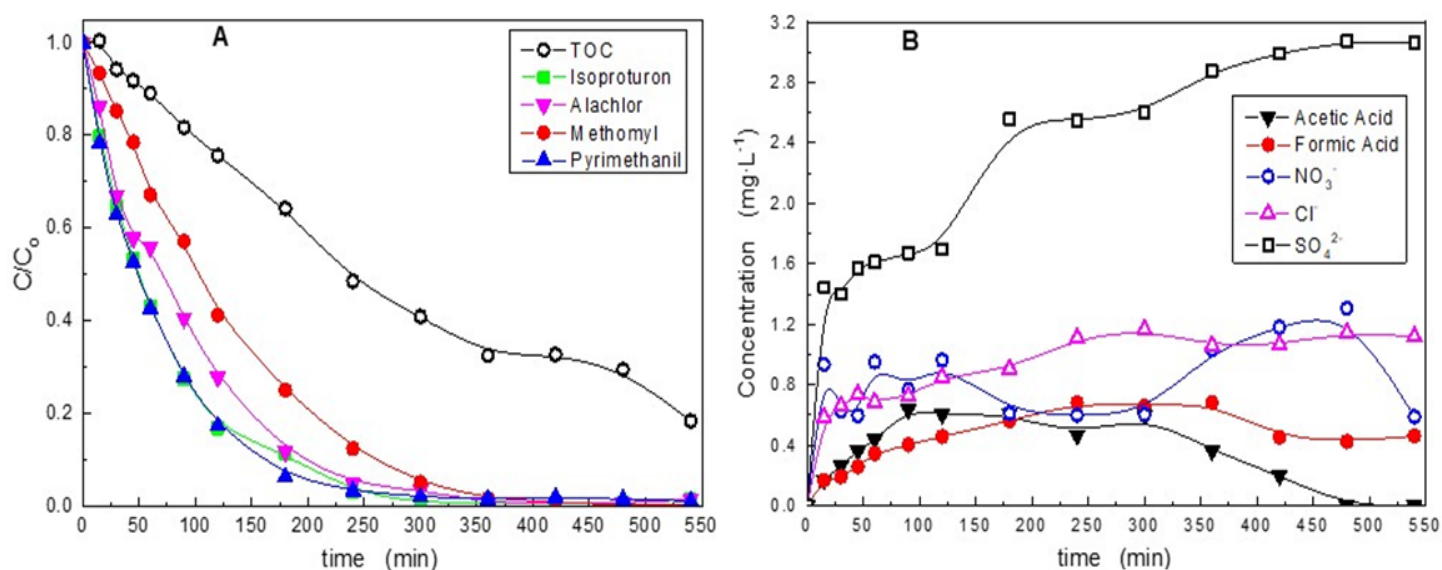
The evolution of pesticides concentration and TOC is shown in **Figures S.11** for these two TiO₂+FLG 0,5% (mortar and sonicated) physical mixed photocatalysts. In both cases, pesticides and TOC conversion rates impressively slowed down (also see **Table 3**), demonstrating the lower photo-efficacy of these two-physical mixed photocatalysts with respect to TiO₂-FLG 0.5 % hybrid nanocomposite. It should be noted the lower pesticides and TOC conversions were always found in the photocatalyst prepared from mortar mixing, even lower than those of the hybrid nanocomposite without FLG, TiO₂-FLG 0.0%. The higher band-gap value (see **Table S.1**), could contribute to mismanage the photon flux leading to fewer photogenerated charges.

Moreover, it can be also emphasized the very low $k_{\text{pesticides}}$ and k_{TOC} , obtained with both physical mixed photocatalysts, especially in the case of mortar mixing photocatalyst, (see **Table 4**).

Table 4. Pseudo-first kinetic constants of pesticides and TOC pseudo-kinetic constants for TiO_2 +FLG 0.50 % mixed photocatalysts and TiO_2 -FLG 0.50 % hybrid nanocomposite.

Nanocomposites	Pesticide								TOC	
	$k_{\text{Isoproturon}}$ (min^{-1})	r^2	$k_{\text{Pyrimethanil}}$ (min^{-1})	r^2	k_{Alachlor} (min^{-1})	r^2	k_{Methomyl} (min^{-1})	r^2	k_{TOC} ($\text{mg}\cdot\text{L}^{-1}\cdot\text{min}^{-1}$)	r^2
TiO_2+FLG 0.50 % - Mortar	0.0049	0.942	0.0074	0.966	0.0063	0.917	0.0035	0.998	0.0146	0.993
TiO_2+FLG 0.50 % - Sonicated	0.0059	0.946	0.0076	0.941	0.0041	0.994	0.0046	0.987	0.0197	0.991
TiO_2-FLG 0.50 % Hybrid nanocomposite	0.0151	0.990	0.0132	0.999	0.0082	0.998	0.0065	0.995	0.0237	0.995

The long term photodegradation efficacy experiment run-up for 9 h was performed with the optimal hybrid photocatalyst, TiO_2 -FLG 0.5 % (**Figures 6**). Where it can be seen all the studied pesticides were completely



Figures 6. Photodegradation of the selected mixture of pesticides with the TiO_2 -FLG 0.5 % hybrid nanocomposite at 550 minutes of irradiation time: (A) Evolution of pesticides and TOC; and (B) Evolution of aromatic intermediates, sulfates, nitrates, and chlorine anions from the photocatalytic degradation of pesticides.

removed at 350 minutes of irradiation time, and around 82 % of TOC conversion was achieved at 540 minutes of irradiation time. Moreover, three different trends can be distinguished in TOC evolution along the photodegradation process. First, TOC evolution showed a steep slope until 350 minutes, where all pesticides were completely removed. Then, TOC halted between 350 and 470 min probably due to the presence of different refractory organic by-products generated during photocatalytic oxidation process,

responsible of the organic matter still present in the reaction medium. And finally, TOC reduction was again addressed to reach remarkable 82% TOC removal.

On the other side, only two short-organic acids were detected, acetic and formic acid, as it can be seen in **Figure 6B**, as final by-products before complete mineralization were achieved, together with some small concentrations of nitrate, chlorine, and higher amounts of sulfate anions, generated from the photocatalytic breakdown of these pesticides.

Finally, delving into the comprehension of the synergistic behavior between FLG and TiO₂ nanoparticles in the hybrid photocatalysts, the role of surface graphitic carbon in the TOC conversion was studied. In **Figure 7**, C data calculated from C-XPS percentage (**Table 1**) and C-XPS deconvolution peak percentage at around 283.9 eV (**Table 2**), has been graphed vs. the corresponding TOC conversions at 300 minutes of irradiation time. A percentage of graphitic carbon in surface around 1.9 % in the TiO₂-FLG 0.5% hybrid nanocomposite has led to the best photoefficiency in the degradation of the pesticides studied here. Moreover, worst TOC values were arisen when C amount on the photocatalyst surface was increased, emphasizing the lowest TOC removal found in the case of TiO₂+FLG 0.5 % - mortar photocatalyst.

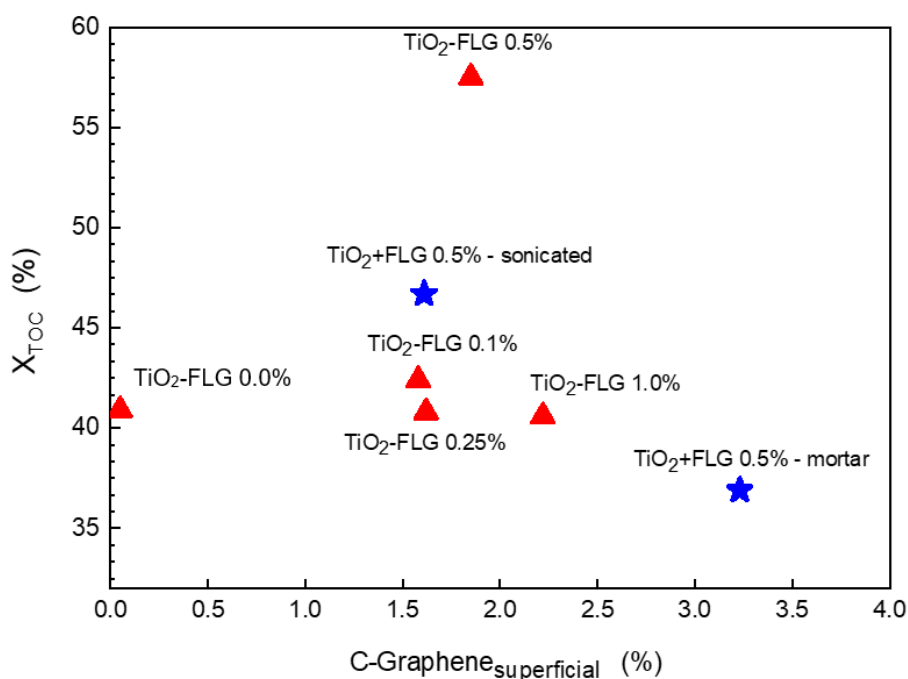


Figure 7. Effect of graphitic carbon in surface (%) on TOC conversions at 300 minutes of irradiation time (▲ TiO₂-FLG hybrid nanocomposites; ★ TiO₂+FLG 0.5% physical mixtures).

Therefore, from the obtained results can be assumed that the junction between titania nanoparticles and FLG is more efficient in the case of hybrid nanocomposites than in the case of physical mixtures, even at the

optimal FLG loading, where a detrimental effect on the pesticides photodegradation was always observed respect to the TiO₂-FLG 0.5 % hybrid nanocomposite.

4. Conclusions

A mechanochemical treatment has been proposed as new ecofriendly methodology to synthesize green titania-graphene nanocomposites for their application in the photocatalytic degradation of a complex mixing of pesticides, classified by EU as priority pollutants (isoproturon, pyrimethanil, alachlor and methomyl).

From XRD patterns all these photocatalysts have presented the same crystal structure with anatase as the main crystalline phase ($\approx 97.5\%$) and brookite as secondary phase ($\approx 2.5\%$).

It can be concluded from EDX and XPS analysis that as the amount of FLG increased, the proportion of titanium and oxygen decreased and the proportion of carbon increased, which indicates that FLG is mainly deposited on the surface of the TiO₂ nanoparticles, wrapping them. Moreover, an interaction between the graphene structure and the TiO₂ nanoparticles can be assumed by Raman spectra results, where it is possible to observe a slight shift in the 2D and G peaks for all the different prepared TiO₂-FLG hybrid nanocomposites and a higher crystalline domain size for TiO₂-FLG-0.5% nanocomposite, without any further annealing step. The best photocatalytic performance in the degradation of pesticides was obtained by TiO₂-FLG 0.5 % hybrid nanocomposite, where all the pesticides were completely removed at 350 minutes, and around 82 % of TOC conversion was achieved at 540 minutes of irradiation time.

Physical mixtures of TiO₂ nanoparticles and 0.5% FLG prepared by mortar or sonication exhibited worst photoefficiency and lower TOC conversion, leading to deduce the existence of pairing synergy balanced between 0.5%FLG and TiO₂, ball milling prepared, where probably the role played by FLG improved charge separation, driving to long-lasting charges which enhance the final photoefficiency.

Whereas a percentage of graphitic carbon in surface around 1.9 % was obtained in the optimal TiO₂-FLG 0.5 % nanocomposite, worst TOC values were arisen when C amount on the photocatalyst surface was increased, emphasizing the lowest TOC removal found in the case of TiO₂+FLG 0.5 % - mortar photocatalyst.

Conflicts of interest

There are no conflicts to declare.

Acknowledgements

Financial support from the EU Graphene-based disruptive technologies, Graphene Flagship core 3 (881603) the Spanish *Ministerio de Economía y Competitividad* (Projects CTQ2017-88158-R and CTQ2015-71238-R (MINECO/FEDER), RTI2018-094958-B-I00 MCIU/AEI/FEDER, UE, Junta *Comunidades de Castilla-La Mancha* (project SBPL4/17/180501/000204) and Junta de Extremadura/FEDER (project GRU18035) are gratefully acknowledged. Beatriz Villajos thanks the Spanish *Ministerio de Economía y Competitividad* for her AEI contract (PRE2019-089049). Raman spectra were collected using a Spectrometer confocal Renishaw InVia Reflex (FEDER-JCCM funding, UNCM13-1E-1663), included in the facilities of the Instituto Regional de Investigación Científica Aplicada (IRICA), which is also acknowledged for technical support. The authors would like to thank Eduardo Prado García Consuegra and Alicia Fraile Chamizo for their technical assistance.

5. References

- [1] A.H. Keihan, R. Hosseinzadeh, M. Farhadian, H. Kooshki, G. Hosseinzadeh, Solvothermal preparation of Ag nanoparticle and graphene co-loaded TiO₂ for the photocatalytic degradation of paraoxon pesticide under visible light irradiation, *RSC Advances*, 6 (2016) 83673-83687.
- [2] M. Syafrudin, R.A. Kristanti, A. Yuniarto, T. Hadibarata, J. Rhee, W.A. Al-Onazi, T.S. Algarni, A.H. Almarri, A.M. Al-Mohaimed, Pesticides in Drinking Water-A Review, *Int J Environ Res Public Health*, 18 (2021).
- [3] E. Castillejos, A. Esteban-Arranz, B. Bachiller-Baeza, I. Rodríguez-Ramos, A. Guerrero-Ruiz, Reductive degradation of 2,4-dichlorophenoxyacetic acid using Pd/carbon with bifunctional mechanism, *Catalysis Today*, (2019).
- [4] S. Khalid, I. Hashmi, S.J. Khan, Bacterial assisted degradation of chlorpyrifos: The key role of environmental conditions, trace metals and organic solvents, *J Environ Manage*, 168 (2016) 1-9.
- [5] S. Ahmed, M.G. Rasul, R. Brown, M.A. Hashib, Influence of parameters on the heterogeneous photocatalytic degradation of pesticides and phenolic contaminants in wastewater: a short review, *J Environ Manage*, 92 (2011) 311-330.
- [6] European Commission (EU). Decision EU 2020/1161.

- [7] J.C.G. Sousa, A.R. Ribeiro, M.O. Barbosa, M.F.R. Pereira, A.M.T. Silva, A review on environmental monitoring of water organic pollutants identified by EU guidelines, *J Hazard Mater*, 344 (2018) 146-162.
- [8] G.R. Echavia, F. Matzusawa, N. Negishi, Photocatalytic degradation of organophosphate and phosphonoglycine pesticides using TiO₂ immobilized on silica gel, *Chemosphere*, 76 (2009) 595-600.
- [9] N.H. Ince, I.G. Apikyan, Combination of activated carbon adsorption with light-enhanced chemical oxidation via hydrogen peroxide, *Water Research*, 34 (2000) 4169-4176.
- [10] R. Andrezzi, Advanced oxidation processes (AOP) for water purification and recovery, *Catalysis Today*, 53 (1999) 51-59.
- [11] D. Ravelli, D. Dondi, M. Fagnoni, A. Albini, Photocatalysis. A multi-faceted concept for green chemistry, *Chem Soc Rev*, 38 (2009) 1999-2011.
- [12] M.N. Chong, B. Jin, C.W. Chow, C. Saint, Recent developments in photocatalytic water treatment technology: a review, *Water Res*, 44 (2010) 2997-3027.
- [13] J. Carbajo, M. Jiménez, S. Miralles, S. Malato, M. Faraldos, A. Bahamonde, Study of application of titania catalysts on solar photocatalysis: Influence of type of pollutants and water matrices, *Chemical Engineering Journal*, 291 (2016) 64-73.
- [14] G. Luna-Sanguino, A. Ruiz-Delgado, A. Tolosana-Moranchel, L. Pascual, S. Malato, A. Bahamonde, M. Faraldos, Solar photocatalytic degradation of pesticides over TiO₂-rGO nanocomposites at pilot plant scale, *Sci Total Environ*, 737 (2020) 140286.
- [15] S. Malato, P. Fernández-Ibáñez, M.I. Maldonado, J. Blanco, W. Gernjak, Decontamination and disinfection of water by solar photocatalysis: Recent overview and trends, *Catalysis Today*, 147 (2009) 1-59.
- [16] C. Haw, W. Chiu, S. Abdul Rahman, P. Khiew, S. Radiman, R. Abdul Shukor, M.A.A. Hamid, N. Ghazali, The design of new magnetic-photocatalyst nanocomposites (CoFe₂O₄-TiO₂) as smart nanomaterials for recyclable-photocatalysis applications, *New Journal of Chemistry*, 40 (2016) 1124-1136.
- [17] E.-H. Kong, J. Lim, J.H. Lee, W. Choi, H.M. Jang, Enhanced photocatalytic activity of {101}-oriented bipyramidal TiO₂ agglomerates through interparticle charge transfer, *Applied Catalysis B: Environmental*, 176-177 (2015) 76-82.
- [18] B. Tryba, Increase of the Photocatalytic Activity of by Carbon and Iron Modifications, *International Journal of Photoenergy*, 2008 (2008) 1-15.

- [19] S. Kwon, M. Fan, A.T. Cooper, H. Yang, Photocatalytic Applications of Micro- and Nano-TiO₂ in Environmental Engineering, *Critical Reviews in Environmental Science and Technology*, 38 (2008) 197-226.
- [20] G. Zerjav, M.S. Arshad, P. Djinovic, I. Junkar, J. Kovac, J. Zavasnik, A. Pintar, Improved electron-hole separation and migration in anatase TiO₂ nanorod/reduced graphene oxide composites and their influence on photocatalytic performance, *Nanoscale*, 9 (2017) 4578-4592.
- [21] S. Wang, D. Li, C. Sun, S. Yang, Y. Guan, H. He, Synthesis and characterization of g-C₃N₄/Ag₃VO₄ composites with significantly enhanced visible-light photocatalytic activity for triphenylmethane dye degradation, *Applied Catalysis B: Environmental*, 144 (2014) 885-892.
- [22] T. Umebayashi, T. Yamaki, H. Itoh, K. Asai, Band gap narrowing of titanium dioxide by sulfur doping, *Applied Physics Letters*, 81 (2002) 454-456.
- [23] H. Yan, X. Wang, M. Yao, X. Yao, Band structure design of semiconductors for enhanced photocatalytic activity: The case of TiO₂, *Progress in Natural Science: Materials International*, 23 (2013) 402-407.
- [24] K.-R. Zhu, M.-S. Zhang, Q. Chen, Z. Yin, Size and phonon-confinement effects on low-frequency Raman mode of anatase TiO₂ nanocrystal, *Physics Letters A*, 340 (2005) 220-227.
- [25] J. Chen, F. Qiu, W. Xu, S. Cao, H. Zhu, Recent progress in enhancing photocatalytic efficiency of TiO₂-based materials, *Applied Catalysis A: General*, 495 (2015) 131-140.
- [26] S. Li, Y. Yang, Q. Su, X. Liu, H. Zhao, Z. Zhao, J. Li, C. Jin, Synthesis and photocatalytic activity of transition metal and rare earth element co-doped TiO₂ nano particles, *Materials Letters*, 252 (2019) 123-125.
- [27] Q.-F. Liu, Q. Zhang, B.-R. Liu, S. Li, J.-J. Ma, Building surface defects by doping with transition metal on ultrafine TiO₂ to enhance the photocatalytic H₂ production activity, *Chinese Journal of Catalysis*, 39 (2018) 542-548.
- [28] S. Kohtani, S. Makino, A. Kudo, K. Tokumura, Y. Ishigaki, T. Matsunaga, O. Nikaido, K. Hayakawa, R. Nakagaki, Photocatalytic Degradation of 4-n-Nonylphenol under Irradiation from Solar Simulator: Comparison between BiVO₄ and TiO₂ Photocatalysts, *Chemistry Letters*, 31 (2002) 660-661.

- [29] A. Nourbakhsh, S. Abbaspour, M. Masood, S.N. Mirsattari, A. Vahedi, K.J.D. Mackenzie, Photocatalytic properties of mesoporous TiO₂ nanocomposites modified with carbon nanotubes and copper, *Ceramics International*, 42 (2016) 11901-11906.
- [30] M. Cruz, C. Gomez, C.J. Duran-Valle, L.M. Pastrana-Martínez, J.L. Faria, A.M.T. Silva, M. Faraldos, A. Bahamonde, Bare TiO₂ and graphene oxide TiO₂ photocatalysts on the degradation of selected pesticides and influence of the water matrix, *Applied Surface Science*, 416 (2017) 1013-1021.
- [31] L. Lin, H. Wang, P. Xu, Immobilized TiO₂-reduced graphene oxide nanocomposites on optical fibers as high performance photocatalysts for degradation of pharmaceuticals, *Chemical Engineering Journal*, 310 (2017) 389-398.
- [32] K. Qi, B. Cheng, J. Yu, W. Ho, A review on TiO₂-based Z-scheme photocatalysts, *Chinese Journal of Catalysis*, 38 (2017) 1936-1955.
- [33] R.A. Doong, C.Y. Liao, Enhanced visible-light-responsive photodegradation of bisphenol A by Cu, N-codoped titanate nanotubes prepared by microwave-assisted hydrothermal method, *J Hazard Mater*, 322 (2017) 254-262.
- [34] X. He, W.G. Aker, M. Pelaez, Y. Lin, D.D. Dionysiou, H.-m. Hwang, Assessment of nitrogen–fluorine-codoped TiO₂ under visible light for degradation of BPA: Implication for field remediation, *Journal of Photochemistry and Photobiology A: Chemistry*, 314 (2016) 81-92.
- [35] C. Chen, Y. Zhang, J. Zeng, F. Zhang, K. Zhou, C.R. Bowen, D. Zhang, Aligned macroporous TiO₂/chitosan/reduced graphene oxide (rGO) composites for photocatalytic applications, *Applied Surface Science*, 424 (2017) 170-176.
- [36] Y. Yu, J.C. Yu, C.-Y. Chan, Y.-K. Che, J.-C. Zhao, L. Ding, W.-K. Ge, P.-K. Wong, Enhancement of adsorption and photocatalytic activity of TiO₂ by using carbon nanotubes for the treatment of azo dye, *Applied Catalysis B: Environmental*, 61 (2005) 1-11.
- [37] A. Dhakshinamoorthy, S. Navalon, A. Corma, H. Garcia, Photocatalytic CO₂ reduction by TiO₂ and related titanium containing solids, *Energy & Environmental Science*, 5 (2012).
- [38] Q. Yang, L. Lu, Q. Xu, S. Tang, Y. Yu, Using Post-graphene 2D Materials to Detect and Remove Pesticides: Recent Advances and Future Recommendations, *Bull Environ Contam Toxicol*, 107 (2021) 185-193.
- [39] A.K. Geim, Graphene: status and prospects, *Science*, 324 (2009) 1530-1534.

- [40] A.K. Geim, K.S. Novoselov, The rise of graphene, *Nat Mater*, 6 (2007) 183-191.
- [41] I.d. Lázaro, S. Vranic, D. Marson, A.F. Rodrigues, M. Buggio, A. Esteban-Arranz, M. Mazza, P. Posocco, K. Kostarelos, Graphene Oxide as 2D Platform for Complexation and Intracellular Delivery of siRNA, (2018).
- [42] B. Kuchta, L. Firlej, A. Mohammadhosseini, P. Boulet, M. Beckner, J. Romanos, P. Pfeifer, Hypothetical high-surface-area carbons with exceptional hydrogen storage capacities: open carbon frameworks, *J Am Chem Soc*, 134 (2012) 15130-15137.
- [43] A. Esteban-Arranz, D. Compte-Tordesillas, V. Muñoz-Andrés, M. Pérez-Cadenas, A. Guerrero-Ruiz, Effect of surface, structural and textural properties of graphenic materials over cooperative and synergetic adsorptions of two chloroaromatic compounds from aqueous solution, *Catalysis Today*, 301 (2018) 104-111.
- [44] X. Huang, X. Qi, F. Boey, H. Zhang, Graphene-based composites, *Chem Soc Rev*, 41 (2012) 666-686.
- [45] F. Zou, Y. Yu, N. Cao, L. Wu, J. Zhi, A novel approach for synthesis of TiO₂-graphene nanocomposites and their photoelectrical properties, *Scripta Materialia*, 64 (2011) 621-624.
- [46] S. Kumari, A. Shekhar, D.D. Pathak, Graphene oxide-TiO₂ composite: an efficient heterogeneous catalyst for the green synthesis of pyrazoles and pyridines, *New Journal of Chemistry*, 40 (2016) 5053-5060.
- [47] Y. Liu, D. Zhang, The preparation of reduced graphene oxide-TiO₂ composite materials towards transparent, strain sensing and photodegradation multifunctional films, *Composites Science and Technology*, 137 (2016) 102-108.
- [48] S. Pu, R. Zhu, H. Ma, D. Deng, X. Pei, F. Qi, W. Chu, Facile in-situ design strategy to disperse TiO₂ nanoparticles on graphene for the enhanced photocatalytic degradation of rhodamine 6G, *Applied Catalysis B: Environmental*, 218 (2017) 208-219.
- [49] C. Lai, M.-M. Wang, G.-M. Zeng, Y.-G. Liu, D.-L. Huang, C. Zhang, R.-Z. Wang, P. Xu, M. Cheng, C. Huang, H.-P. Wu, L. Qin, Synthesis of surface molecular imprinted TiO₂/graphene photocatalyst and its highly efficient photocatalytic degradation of target pollutant under visible light irradiation, *Applied Surface Science*, 390 (2016) 368-376.
- [50] Y. Zhang, N. Zhang, Z.R. Tang, Y.J. Xu, Improving the photocatalytic performance of graphene-TiO₂ nanocomposites via a combined strategy of decreasing defects of graphene and increasing interfacial contact, *Phys Chem Chem Phys*, 14 (2012) 9167-9175.

- [51] Y. Zhang, Z.R. Tang, X. Fu, Y.J. Xu, Engineering the unique 2D mat of graphene to achieve graphene-TiO₂ nanocomposite for photocatalytic selective transformation: what advantage does graphene have over its forebear carbon nanotube?, *ACS Nano*, 5 (2011) 7426-7435.
- [52] Y. Zhang, Z.R. Tang, X. Fu, Y.J. Xu, TiO₂-graphene nanocomposites for gas-phase photocatalytic degradation of volatile aromatic pollutant: is TiO₂-graphene truly different from other TiO₂-carbon composite materials?, *ACS Nano*, 4 (2010) 7303-7314.
- [53] C. Basheer, Application of Titanium Dioxide-Graphene Composite Material for Photocatalytic Degradation of Alkylphenols, *Journal of Chemistry*, 2013 (2013) 1-10.
- [54] D.A.H. Hanaor, C.C. Sorrell, Review of the anatase to rutile phase transformation, *Journal of Materials Science*, 46 (2010) 855-874.
- [55] Q. Xiang, J. Yu, M. Jaroniec, Graphene-based semiconductor photocatalysts, *Chem Soc Rev*, 41 (2012) 782-796.
- [56] W. Han, L. Ren, L. Gong, X. Qi, Y. Liu, L. Yang, X. Wei, J. Zhong, Self-Assembled Three-Dimensional Graphene-Based Aerogel with Embedded Multifarious Functional Nanoparticles and Its Excellent Photoelectrochemical Activities, *ACS Sustainable Chemistry & Engineering*, 2 (2014) 741-748.
- [57] G. Liao, D. Zhu, J. Zheng, J. Yin, B. Lan, L. Li, Efficient mineralization of bisphenol A by photocatalytic ozonation with TiO₂-graphene hybrid, *Journal of the Taiwan Institute of Chemical Engineers*, 67 (2016) 300-305.
- [58] G. Williams, B. Seger, P.V. Kamat, TiO₂-graphene nanocomposites. UV-assisted photocatalytic reduction of graphene oxide, *ACS Nano*, 2 (2008) 1487-1491.
- [59] T.N. Lambert, C.A. Chavez, B. Hernandez-Sanchez, P. Lu, N.S. Bell, A. Ambrosini, T. Friedman, T.J. Boyle, D.R. Wheeler, D.L. Huber, Synthesis and Characterization of Titania-Graphene Nanocomposites, *The Journal of Physical Chemistry C*, 113 (2009) 19812-19823.
- [60] D. Wang, D. Choi, J. Li, Z. Yang, Z. Nie, R. Kou, D. Hu, C. Wang, L.V. Saraf, J. Zhang, I.A. Aksay, J. Liu, Self-assembled TiO₂-graphene hybrid nanostructures for enhanced Li-ion insertion, *ACS Nano*, 3 (2009) 907-914.
- [61] H. Zhang, X. Lv, Y. Li, Y. Wang, J. Li, P25-graphene composite as a high performance photocatalyst, *ACS Nano*, 4 (2010) 380-386.

- [62] Y. Liang, H. Wang, H. Sanchez Casalongue, Z. Chen, H. Dai, TiO₂ nanocrystals grown on graphene as advanced photocatalytic hybrid materials, *Nano Research*, 3 (2010) 701-705.
- [63] N. Yang, J. Zhai, D. Wang, Y. Chen, L. Jiang, Two-dimensional graphene bridges enhanced photoinduced charge transport in dye-sensitized solar cells, *ACS Nano*, 4 (2010) 887-894.
- [64] I.V. Lightcap, T.H. Kosel, P.V. Kamat, Anchoring semiconductor and metal nanoparticles on a two-dimensional catalyst mat. Storing and shuttling electrons with reduced graphene oxide, *Nano Lett*, 10 (2010) 577-583.
- [65] D. Chen, H. Zhang, Y. Liu, J. Li, Graphene and its derivatives for the development of solar cells, photoelectrochemical, and photocatalytic applications, *Energy & Environmental Science*, 6 (2013).
- [66] A. Tayel, A. Ramadan, O. El Seoud, Titanium Dioxide/Graphene and Titanium Dioxide/Graphene Oxide Nanocomposites: Synthesis, Characterization and Photocatalytic Applications for Water Decontamination, *Catalysts*, 8 (2018).
- [67] A. Giampiccolo, D.M. Tobaldi, S.G. Leonardi, B.J. Murdoch, M.P. Seabra, M.P. Ansell, G. Neri, R.J. Ball, Sol gel graphene/TiO₂ nanoparticles for the photocatalytic-assisted sensing and abatement of NO₂, *Applied Catalysis B: Environmental*, 243 (2019) 183-194.
- [68] L.C. Chen, C.H. Hsu, P.S. Chan, X. Zhang, C.J. Huang, Improving the performance of dye-sensitized solar cells with TiO₂/graphene/TiO₂ sandwich structure, *Nanoscale Res Lett*, 9 (2014) 380.
- [69] Y. Jiang, W.N. Wang, P. Biswas, J.D. Fortner, Facile aerosol synthesis and characterization of ternary crumpled graphene-TiO₂-magnetite nanocomposites for advanced water treatment, *ACS Appl Mater Interfaces*, 6 (2014) 11766-11774.
- [70] M.A. Fitri, M. Ota, Y. Hirota, Y. Uchida, K. Hara, D. Ino, N. Nishiyama, Fabrication of TiO₂-graphene photocatalyst by direct chemical vapor deposition and its anti-fouling property, *Materials Chemistry and Physics*, 198 (2017) 42-48.
- [71] A. Datcu, M.L. Mendoza, A.P. del Pino, C. Logofatu, C. Luculescu, E. György, UV-vis light induced photocatalytic activity of TiO₂/graphene oxide nanocomposite coatings, *Catalysis Today*, 321-322 (2019) 81-86.
- [72] F.W. Low, C.W. Lai, Recent developments of graphene-TiO₂ composite nanomaterials as efficient photoelectrodes in dye-sensitized solar cells: A review, *Renewable and Sustainable Energy Reviews*, 82 (2018) 103-125.

- [73] M. Faraldos, A. Bahamonde, Environmental applications of titania-graphene photocatalysts, *Catalysis Today*, 285 (2017) 13-28.
- [74] D.J. Li, Z. Huang, T.H. Hwang, R. Narayan, J.W. Choi, S.O. Kim, Atomic thin titania nanosheet-coupled reduced graphene oxide 2D heterostructures for enhanced photocatalytic activity and fast lithium storage, *Electronic Materials Letters*, 12 (2016) 211-218.
- [75] S.M.-T. L. M. Pastrana-Martínez, A. G. Kontos, N. G. Moustakas, J. L. Faria, J. M. Doña-Rodríguez, P. Falaras, A. M. T. Silva, Nanostructured carbon-TiO₂ photocatalysts for water purification: an overview, *Chem. Eng. J.*, 224 (2013) 17-23.
- [76] J.M. Gonzalez-Dominguez, V. Leon, M.I. Lucio, M. Prato, E. Vazquez, Production of ready-to-use few-layer graphene in aqueous suspensions, *Nat Protoc*, 13 (2018) 495-506.
- [77] V. Leon, J.M. Gonzalez-Dominguez, J.L. Fierro, M. Prato, E. Vazquez, Production and stability of mechanochemically exfoliated graphene in water and culture media, *Nanoscale*, 8 (2016) 14548-14555.
- [78] L. Takacs, What Is Unique About Mechanochemical Reactions?, *Acta Physica Polonica A*, 126 (2014) 1040-1043.
- [79] K.G. K. Wiecek-Ciurowa, Some aspects of mechanochemical reactions, *Materials Science Poland* 25 (2007) 219-232.
- [80] P. Wang, C. Qi, P. Wen, L. Hao, X. Xu, S. Agathopoulos, Synthesis of Si, N co-Doped Nano-Sized TiO₂ with High Thermal Stability and Photocatalytic Activity by Mechanochemical Method, *Nanomaterials (Basel)*, 8 (2018).
- [81] B.D.C.S.R. Stock, *Elements Of X-ray Diffraction*, 3rd ed., 2001.
- [82] H.N.D. Z. Chen, *E. Miller Photoelectrochemical Water Splitting: Standards, Experimental Methods, and Protocols*, Springer, 2013.
- [83] A. Tolosana-Moranchel, J.A. Casas, A. Bahamonde, L. Pascual, L.I. Granone, J. Schneider, R. Dillert, D.W. Bahnemann, Nature and photoreactivity of TiO₂-rGO nanocomposites in aqueous suspensions under UV-A irradiation, *Applied Catalysis B: Environmental*, 241 (2019) 375-384.
- [84] P. García-Muñoz, J. Carbajo, M. Faraldos, A. Bahamonde, Photocatalytic degradation of phenol and isoproturon: Effect of adding an activated carbon to titania catalyst, *Journal of Photochemistry and Photobiology A: Chemistry*, 287 (2014) 8-18.

- [85] W.F. Zhang, Y.L. He, M.S. Zhang, Z. Yin, Q. Chen, Raman scattering study on anatase TiO₂ nanocrystals, *Journal of Physics D: Applied Physics*, 33 (2000) 912-916.
- [86] D. Georgescu, L. Baia, O. Ersen, M. Baia, S. Simon, Experimental assessment of the phonon confinement in TiO₂ anatase nanocrystallites by Raman spectroscopy, *Journal of Raman Spectroscopy*, 43 (2012) 876-883.
- [87] A.C. Ferrari, Raman spectroscopy of graphene and graphite: Disorder, electron-phonon coupling, doping and nonadiabatic effects, *Solid State Communications*, 143 (2007) 47-57.
- [88] V. Swamy, A. Kuznetsov, L.S. Dubrovinsky, R.A. Caruso, D.G. Shchukin, B.C. Muddle, Finite-size and pressure effects on the Raman spectrum of nanocrystalline anatase TiO₂, *Physical Review B*, 71 (2005).
- [89] S. Kelly, F.H. Pollak, M. Tomkiewicz, Raman Spectroscopy as a Morphological Probe for TiO₂ Aerogels, *The Journal of Physical Chemistry B*, 101 (1997) 2730-2734.
- [90] B. Tang, H. Guoxin, H. Gao, Raman Spectroscopic Characterization of Graphene, *Applied Spectroscopy Reviews*, 45 (2010) 369-407.
- [91] T. Bezrodna, G. Puchkovska, V. Shymanovska, J. Baran, H. Ratajczak, IR-analysis of H-bonded H₂O on the pure TiO₂ surface, *Journal of Molecular Structure*, 700 (2004) 175-181.
- [92] A. Tolosana-Moranchel, J.A. Casas, J. Carbajo, M. Faraldos, A. Bahamonde, Influence of TiO₂ optical parameters in a slurry photocatalytic reactor: Kinetic modelling, *Applied Catalysis B: Environmental*, 200 (2017) 164-173.
- [93] R. Scotti, M. D'Arienzo, A. Testino, F. Morazzoni, Photocatalytic mineralization of phenol catalyzed by pure and mixed phase hydrothermal titanium dioxide, *Applied Catalysis B: Environmental*, 88 (2009) 497-504.
- [94] V. Augugliaro, M. Bellardita, V. Loddo, G. Palmisano, L. Palmisano, S. Yurdakal, Overview on oxidation mechanisms of organic compounds by TiO₂ in heterogeneous photocatalysis, *Journal of Photochemistry and Photobiology C: Photochemistry Reviews*, 13 (2012) 224-245.
- [95] K.V. Kumar, K. Porkodi, F. Rocha, Langmuir-Hinshelwood kinetics – A theoretical study, *Catalysis Communications*, 9 (2008) 82-84.
- [96] Á. Tolosana-Moranchel, A. Manassero, M.L. Satuf, O.M. Alfano, J.A. Casas, A. Bahamonde, Influence of TiO₂-rGO optical properties on the photocatalytic activity and efficiency to photodegrade an emerging pollutant, *Applied Catalysis B: Environmental*, 246 (2019) 1-11.

